THERMAL AND SPECTROSCOPIC INVESTIGATIONS OF COMPLEXES OF THE SELECTED TRANSITION METAL IONS WITH A *β*-L-ASPARTYL AMIDE DERIVATIVE

Carmen SACALIS[a,*], Igballe ABDIJI[b], Maria DAVID[c], Ahmed JASHARI[b]

ABSTRACT. The aim of the presented research was to synthesize and characterize *via* elemental analysis, HRMS, thermogravimetric analysis, FTIR and EPR a novel series of transition metal complexes of Cu(II), Co(II), Ni(II) and Mn(II) with *β*-L-aspartyl-cyclohexyl amide as ligand. The HRMS recorded spectra confirm the obtaining of new compounds. The changes in the FTIR spectra of the metal complexes, compared to the ligand, support the complexation process. The thermal stability of the ligand and its metal complexes was discussed in the 20-800^{0}C temperature range, in air atmosphere. In all of the studied complexes, the aspartyl amide acts as a bidentate ligand, its coordination involving the carboxylate oxygen and the nitrogen atom belonging to the free amino group of the amino acid. Metal complexes are formed in the 1:2 (Metal:Ligand) ratio as found by the elemental analysis. Except the free ligand, all the metal complexes are hydrating with water molecules, and the thermal stability of these suggested whether the water molecules are inside or outside the coordination sphere. The shape of EPR spectrum for copper complex at room temperature suggests the presence of CuN_2O_2 monomeric species with a rhombic distortion around the metallic ion. The results indicate that their stability range obeys the Irving-Williams series.

Keywords: *L-aspartic acid, aspartyl amide, metal complexes, thermal behavior, spectroscopic studies*

[a] *Babeş-Bolyai University, Faculty of Chemistry and Chemical Engineering, 11 Arany Janos Str., RO-400028, Cluj-Napoca, Romania*
[b] *University of Tetova, Faculty of Natural Sciences and Mathematics, Bldv.Ilinden, nn., 1200 Tetova, Republic of North Macedonia*
[c] *National Institute for Research and Development of Isotopic and Molecular Technologies, 67-103 Donath str. RO-400293, Cluj-Napoca, Romania*
* Corresponding author carmen.sacalis@ubbcluj.ro

INTRODUCTION

L-aspartic acid is one of the 22 proteinogenic amino acids, that is used in the biosynthesis of proteins. It is a metabolite in the urea cycle and participates in gluconeogenesis. L-aspartic acid is a naturally-occurring amino acid and a component of the active center of some enzymes. Due to its biological importance L-aspartic acid or peptide containing aspartyl residue was chosen in a lot of complexation products [1-6].

Coordination compounds of amino acids, including aspartic acid, demonstrate an activity varying from marginal to significantly good antimicrobial properties. As a result of resistance to the drugs currently in use and the emergence of new diseases, there is a continuous need for the synthesis and identification of new compounds as potential antimicrobial agents. Metal complexes of aspartic acid with Cu(II), Co(II), Ni(II), Cd(II) or Mn(II) demonstrate antimicrobial activities against Gram-positive, Gram-negative bacteria or fungus [7].

Polymeric silver (I) complex with aspartic acid or asparagine showed a wide spectrum of antimicrobial activities against *E. coli, P. aeruginosa, B. subtilis, S. aureus, C. albicans and S. cerevisiae* [8].

L-aspartic acid contained in some biodegradable polyesters was tested as drug delivery in the cancer cell line with promises results [2].

Surfactants derived from amino and α-hydroxy acids were synthesized and tested for aquatic toxicity. Amide and ester derivatives of C_{10}-C_{16} fatty acids with amino acids, including aspartic acid or α-hydroxy acids such as malic or citric acid, were synthetized and tested for potential aquatic toxicity using zebrafish larvae as experimental animals. The reported results indicated that all the surfactants derived from natural products can be classified as environmentally benign [9].

Mixed metal complexes of L-aspartic acid and *o*-phenanthroline with rare earth such as La(III), Eu(III), Tb(III), Dy(III) and Y(III) showed a strong inhibitory effect on *E.coli, S. aureus* and *C. albicans*, and a considerable destructive effect on cancer cells [10].

Recently, a theoretical study proposed the amino acids, including L-aspartic acid and L- asparagine, as a chelating agents to remove heavy metal cations like Cd^{2+}, Cu^{2+}, Ni^{2+}, Hg^{2+}, Zn^{2+}, Mn^{2+} and Fe^{3+} could represent a good way to reduce the metal pollution in soil and environments [11].

New macrocyclic ligand and its Mn(II) and Cu(II) nanocomplexes from macrocycles containing amide groups using L-aspartic acid and ethylene diamine was reported. The obtained results indicate that the complexes can act as a promising candidate as green emitting light materials in electroluminescent and optoelectronic devices. Antimicrobial studies showed that Cu(II) complex acts as an antimicrobial agent against fungal strains and Gram-positive or Gram-negative bacteria [12].

We previously reported the convenient preparation of β-L-aspartyl-cyclohexyl amide (Figure 1) as a potential ligand for transition metal complexes by an original method which involved 4 steps of synthesis, using *N*-carbethoxyphthalimide as protective amino reagent *via* a mild phthaloylation [13].

On the basis of the above results, we explored the synthesis, with thermal and spectroscopic investigations of Cu(II), Co(II), Ni(II) and Mn(II) and with aforementioned β-L-aspartyl amide as ligand. All these compounds were analyzed by spectral analysis (HRMS, FT-IR and EPR) and thermal studies. The results are in good agreement with the thermal stability range and obeys the Irving-Williams series [14].
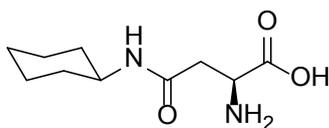
Figure 1. Structure formula of ligand (*S*)-2-amino-4-(cyclohexyl amino)-4-oxobutanoic acid (**HL**) or (**1**)

The objective of this study was to synthesize and analyze a new series of metal complexes of selected transition metal ions such as: Cu(II), Co(II), Ni(II), and Mn(II), using an aspartic acid amide as the organic ligand, previously prepared by our team, using a novel, more efficient method than those reported in the literature. Given that many drugs are administered in the form of metal complexes, we also conducted a study on their thermal behavior and stability upon heating, which could open new opportunities for testing these compounds in the medical field.

RESULTS AND DISCUSSION

The structure of the metal complexes

The complexation reaction of metal salts occurs in mild conditions and, in each case, yields a solid product. All the complexes are stable at room temperature. In our experiments, the metal complexes obtained as colored microcrystalline powder are characterized by elemental analysis, mass spectra, infrared spectral data, thermal studies and EPR data. Higher melting points of these products, as well their different colors when compared to that of the ligand, indicate the formation of metal complexes. Thermal analysis allowed us to evaluate the assumed position of crystallization water molecules in outer or inner spheres of complex coordination and determine the endo- or exothermic effects connected with each process such as dehydration, melting,

decarboxylation, fragmentation and finally pyrolysis of the organic rest. The EPR spectra gave us information about the local symmetry around the metal ions, especially in the case of the copper complex.
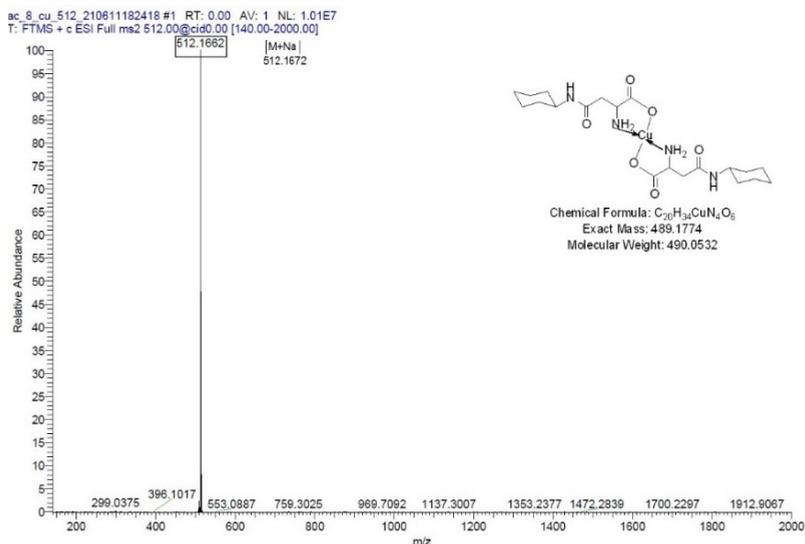

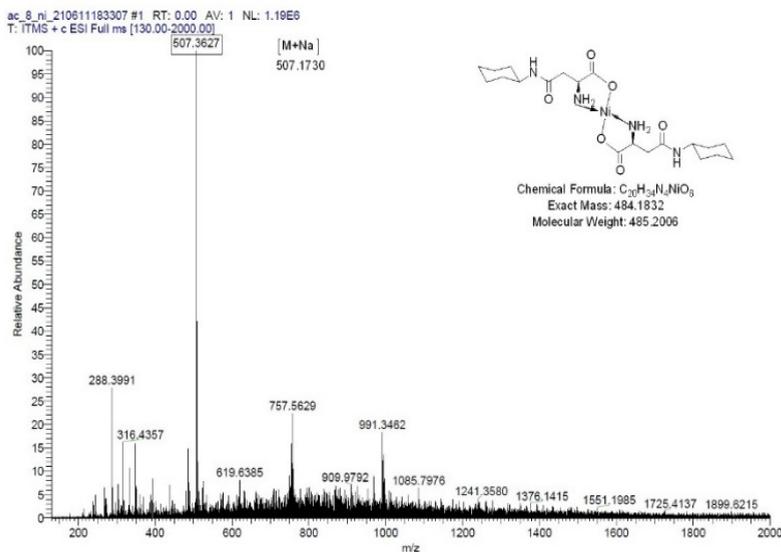**Figure 2a.** HRMS spectrum (ESI) of copper complex (2)

Figure 2b. HRMS spectrum (ESI) of nickel complex (4)

Another proof of the complexation is the HRMS spectrum for the metal complexes (Figure 2a-b). A peak of the highest intensity (100%), corresponding to the [M+Na]$^+$, supports the complexation idea with the transition metal ions, for each of the compounds.

Their elemental analysis data is in good agreement with the molar ratio Metal:Ligand=1:2, which indicates that the aspartyl amide acts as a bidentate ligand, its coordination involving the carboxyl group and the nitrogen atom belonging to the amino group of the aspartic acid fragment, fact also found in the case of other amino acid residues [7, 15-20]. As a result of elemental analysis, it was found that the ligand is anhydrous, but the metal complexes are hydrated, fact that is also confirmed by the thermal analysis data.

Infrared spectra

The FTIR spectra for the ligand and its metal complexes were recorded in the solid state in the wavenumber range of 400-4000cm^{-1} with the aim of highlighting the $v_{(M-O)}$ and $v_{(M-N)}$ stretching vibrations, specific to metallic complexes. The IR spectra provide valuable information regarding the nature of the functional group attached to the metal atom.

Partial assignments of the IR absorption bands, observed for the free ligand and its transition metal complexes, are given in Table 1.

**Table 1.** Selected IR data (cm^{-1}) of the ligand (HL) and its metal complexes (2-5)

Compound	$C_{10}H_{18}N_2O_3$ HL (1)	$C_{20}H_{36}CuN_4O_7$ [Cu(L)$_2$]•H$_2$O (2)	$C_{20}H_{38}CoN_4O_8$ [Co(L)$_2$•2H$_2$O] (3)	$C_{20}H_{38}N_4NiO_8$ [Ni(L)$_2$•2H$_2$O] (4)	$C_{20}H_{38}MnN_4O_8$ [Mn(L)$_2$]•2H$_2$O (5)
v(O-H)	3445(bb)	3423(bb)	3329(bb)	3339(bb)	3407(bb)
v(NH$_2$)	3296(s)	3257(s)	3297(s)	3295(m)	signal covered by broadband
v(CH$_2$as) from cyclohexyl ring	2930(vs)	2930(vs)	2930(s)	2936(s)	2927(w)
v(CH$_2$sym) from cyclohexyl ring	2853(s)	2854(m)	2854(m)	2854(m)	2852(w)
v(COO$^-$as)	1658(s)	1651(vs)	1650(vs)	1650(s)	1556(m)
δ(NH)	1620(vs)	1589(vs)	1622(vs)	1573(vs)	1526(s)
v(COO$^-$sym)	1574(s)	1561(vs)	1558(vs)	1588(s)	1511(vs)
δ(CH$_2$) from cyclohexyl ring	1429(vs)	1405(m)	1404(s)	1418(m)	1407(m)
v(NH)	1310(m)	1367(m)	1389(m)	1312(m)	1373(vs)
v(M-N)	-	588(m)	531(m)	562(m)	457(w)
v(M-O)	-	469(m)	396(w)	423(w)	373(m)

w: weak; m: medium; s: strong; vs: very strong; bb: broadband

The bonding of the ligand to different transition metal ions was investigated also by comparing the IR spectrum of the free ligand (1) with those of the metal complexes (2-5) (Figure 3).

In the spectral region of 3300-3450 cm^{-1} a broadband formed by some overlapped bands is observed, that may be assigned to v_{O-H} vibration due to intra- and intermolecular hydrogen bonding in the crystalline state. The broad envelope band with higher intensity in all those complexes could indicate the presence of weak hydrogen bonds that stabilize the structure of the metal compounds [16-17, 21].

For the ligand a smaller, but broad band at 3445 cm^{-1} (Lit. [22], 3424cm^{-1}), was assigned to the $v(O-H)$ from carboxylic group [22-23]. The fact that the ligand is anhydrous can also be seen from the shape of the band which is smaller compared to the metal complexes. The intense board absorption band at 3339-3423 cm^{-1} in the metal compounds indicates the presence of water molecules [24-25].
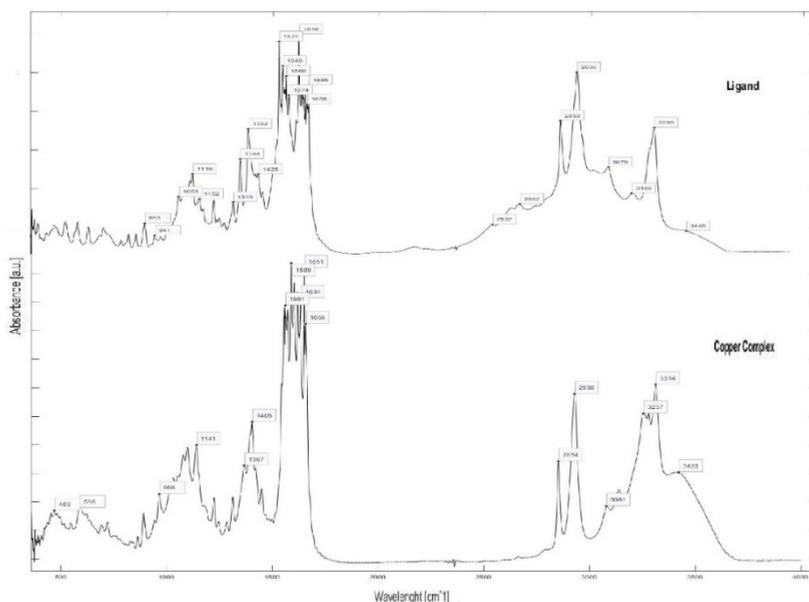
**Figure 3.** IR spectra of the ligand (1) and its copper complex (2)

The vibrational frequencies related to $v(COO^-as)$ at 1658 cm^{-1} (Lit. [26] at 1658 cm^{-1} and Lit. [22] at 1637 cm^{-1}) and $v(COO^-sym)$ at 1574 cm^{-1} (Lit. [26] at 1570 cm^{-1} and Lit. [22] at 1598 cm^{-1}) in ligand, is shifted toward lower value in the IR spectra of the compounds (2-5) after complexation. Also, the $v(NH_2)$ and $\delta(NH)$ frequencies in the metal complexes were shifted to lower value due to chelating with metal ions [7, 27].

The $v(CH_2as)$ and $v(CH_2sym)$ corresponding to the cyclohexyl ring keep roughly the same value. New bands in the spectra of the transition metal complexes at 457-588 cm^{-1} were assigned to $v(M\text{-}N)$ stretching frequencies. The participation of the lone pair of electrons on the N of the amino group in the ligand in coordination is supported by these bands. On the other hand, the bands in the region of 373-469 cm^{-1} indicate the formation of M-O bond as a result of the coordination of the ligand to the central metal ions *via* the oxygen atom of the carboxylate rest. This band was assigned to $v(M\text{-}O)$ stretching frequencies, as similar to other metal complexes [7,12, 27-30].

The $v(M\text{-}N)$ and $v(M\text{-}O)$ stretching bands are shifted progressively to higher frequencies as the metal is changed in the order:

Mn(II) < Co(II) < Ni(II) < Cu(II)
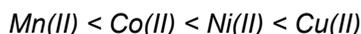
in good agreement with Nakamoto predictions for the amino acid complexes [27]. The shifts are dependent on the metal ions and the magnitudes of shifts follow the Irving-Williams series [14].

Thermal analysis

The thermal behavior of the ligand and its metal complexes was performed in air atmosphere in order to study the nature of water in the investigated compounds, their thermal stability, as well as decomposition modes under controlled heating rate. The analysis of the thermogravimetric curves demonstrates that, both for the ligand as well as for the metal compounds, they undergo gradual decomposition as the temperature increases.
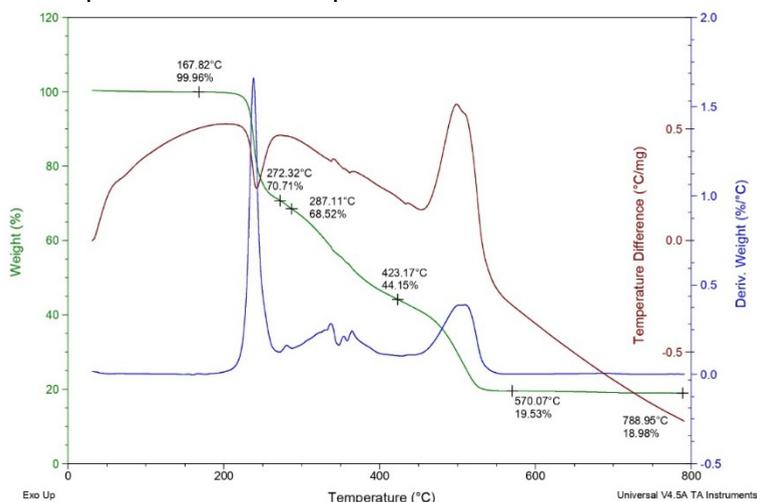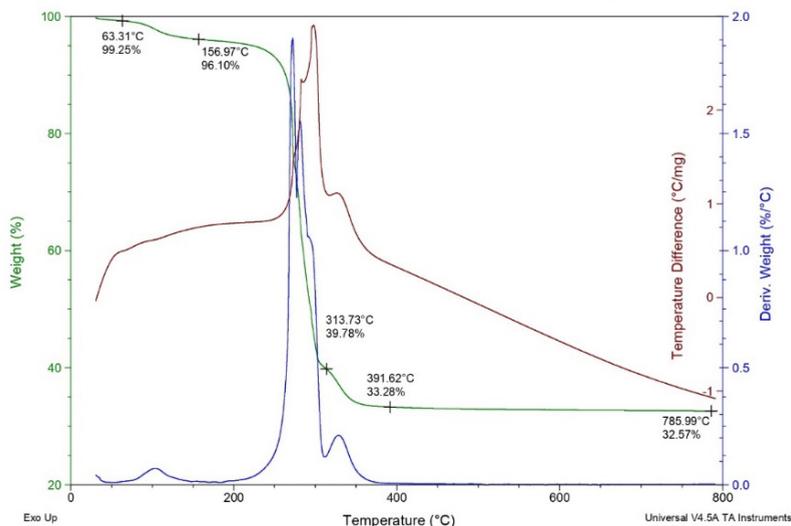

Figure 4a. TG-DTG-DTA diagram for the ligand (1)

The thermal behavior of the ligand (HL) or (1) and its metal complexes (2-5) are summarized in Table 2 and Figure 4a-e.

Thermal decomposition of the ligand (1) was achieved in three stages. The thermal analysis data, in good agreement with those of the elemental analysis, indicate that the ligand is anhydrous, so the small endothermic peak at 168^0C on DTA curve and a mass loss of only 0.04% corresponds to the water present in the air atmosphere. An endothermic peak at 231^0C and an exothermic peak at 272^0C was associated with a melting with decomposition.

The decarboxylation of the amino acid rest and degradation of the free amino group, with loss of a fragment ($-CH_3O_2N$) probably occurs in this stage. The experimental mass loss is 29.25%, close value to the calculated data of 28.48%. This violent burning process of the organic rest, as seen in the DTG curve, is generally specific to compounds with a high oxygen and nitrogen content [19, 31]. The second stage of decomposition occurs within the temperature range of $278-423^0C$, being accompanied by a large board on DTA curve. Three exothermic peaks at 339^0C, 356^0C and 371^0C, respectively with an experimental mass loss of 24.37% (calcd. 25.69%) can be noted in this stage. It is expected to take place a new fragmentation of the organic rest, at the amidic bond and loss of a $-C_3H_4O$ radical. The last stage begins at 423^0C and is associated with a continuous degradation of the sample. The maximum mass loss for the three stages is at 489^0C. As can be seen in the Figure 4a, the organic compound is completely pyrolyzed until 570^0C, finally some ash remaining in the crucible.

Figure 4b. TG-DTG-DTA diagram for the copper complex (2)

The aim of the thermal analysis of the metal complexes is to obtain information concerning their thermal stability and to decide whether the water molecules are inside or outside the coordination sphere [17-19].

For the thermal investigation of copper complex, a sample of 3.5790 mg was taken (Figure 4b). When heated, the complex starts to decompose at 104^0C and loses one water molecule outside coordination sphere in the temperature range of 20-186^{0}C. This phenomenon is connected with an endothermic peak and a mass loss of 3.15% (calcd. 3.54%). The first endothermic peak at 63^{0}C can be assigned to the moisture in the air and inside pores of the substance. In the second step, the metal complex is releasing partially organic ligand with a strong exothermic effect and a great mass loss of 56.32% (calcd. 58.13%). Three exothermic peaks at 271^{0}C, 279^{0}C and 296^{0}C respectively, confirm this fragmentation process. Probably decarboxylation, the amidic split and the amino group degradation accompanies this step. The violent decomposition of the anhydrous complex is often encountered in the case of copper complexes [24]. The third-stage decomposition takes place at 307-400^{0}C with a small exothermic peak at 392^{0}C, corresponding to the pyrolysis of organic rest and formation, ultimately, of CuO.
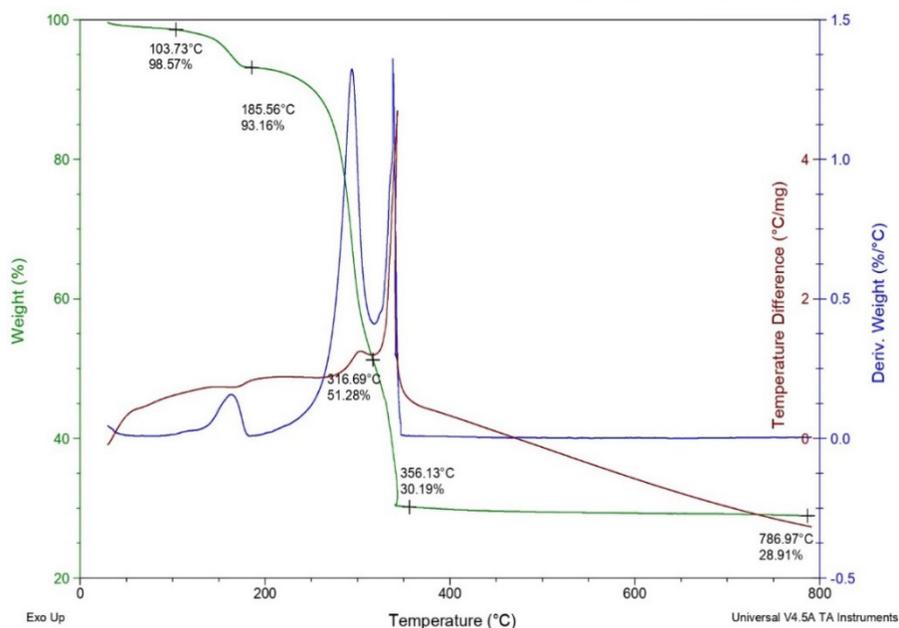
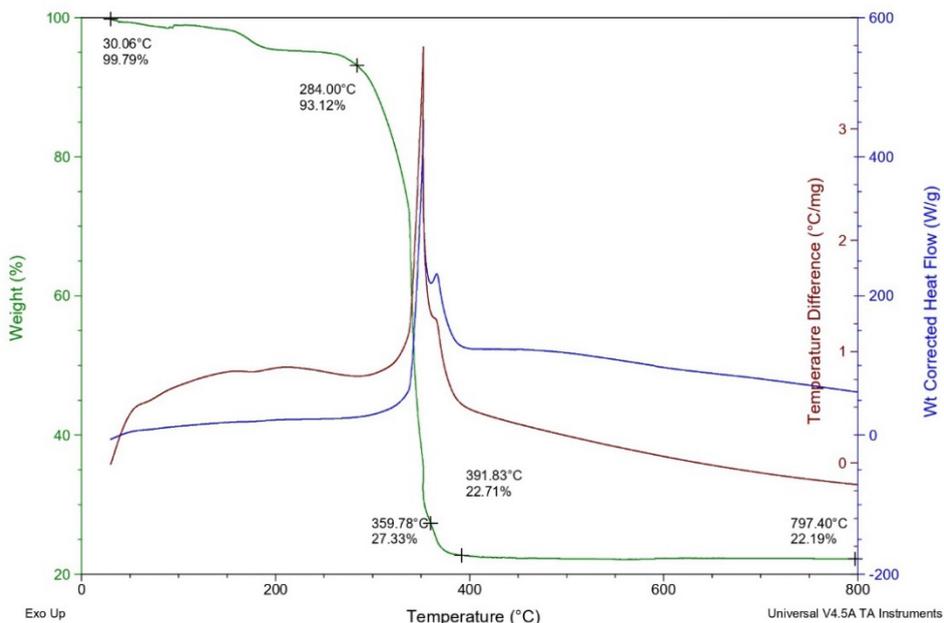**Figure 4c.** TG-DTG-DTA diagram for the cobalt complex (3)

The thermal decomposition of the cobalt complex also occurs in three stages (Figure 4c). The first stage decomposition starts in the temperature range of 20-186^{0}C, with a mass loss of 6.84% (calcd. 6.90%), which corresponds to the loss of 2 mole of water. The higher temperature, 164^{0}C, is an indication that the water is inside the coordination sphere of the metal complex.

Table 2. Thermo-gravimetric data of the ligand (HL) and its metal complexes (2-5)

Compd.	Stage	Heat effect on DTA	Temperature (^{0}C)			Mass loss (%)		Assignment
			T_i	T_{max}	T_f	Calcd.	Experim.	
HL	I	Endo	20	168	278	-	0.04	-residual water
(1)		Endo		231				
		Exo		272		28.48	29.25	-melting with decomp.
	II	Exo	278	339	423			-fragmentation the organic
		Exo		356				rest at the amidic bond
		Exo		371		25.69	24.37	-pyrolysis of organic rest
	III	Exo	423	489	570			-ash residue
		Exo		570			26.81	
						45.83	19.53	
[Cu(L)$_2$]•H$_2$O	I	Endo	20	63	186	-	0.75	-residual water
(2)		Endo		104		3.54	3.15	-1 mole of water
	II	Exo	186	271	307			- fragmentation the organic
		Exo		279				rest
		Exo		296		58.13	56.32	
	III	Exo	307	392	400		6.50	-pyrolysis of organic rest
						38.33	33.28	ash and CuO residue
[Co(L)$_2$•2H$_2$O]	I	Endo	20	32	186	-	1.43	-residual water
(3)		Endo		164		6.90	5.41	-2 mole of water
	II	Endo	186	275	317	-	-	-melting point with
								decompose
		Exo		303		42.90	41.88	-decomp. of ligand
	III	Exo	317	356	400	29.93	30.19	pyrolysis of organic rest
								-ash and CoO
						20.27	21.09	
[Ni(L)$_2$•2H$_2$O]	I	Endo	20	175	284	6.91	6.88	-2 mole of water
(4)	II	Exo	284	360	392	66.96	65.79	-total pyrolysis of metal
								complex
						26.13	27.33	-ash and NiO
[Mn(L)$_2$]•2H$_2$O	I	Endo	20	97	191	6.96	6.69	-2 mole of water
(5)	II	Exo	191	243	371		3.40	-gradually decomposition
		Exo		354			14.99	of organic rest
	III	Exo	371	389	475	24.93	7.2	
	IV	Exo	475	532	768		3.01	
		Exo		643			1.22	
						39.18	36.51	
						28.93	26.98	-ash and MnO

The second stage of decomposition was observed in the 186-317^{0}C range. A small endothermic peak at 275^{0}C can be assigned to the melting point with decompose, and an exothermic peak at 303^{0}C, with an experimental mass loss of 42.90% (calcd. 41.88%), corresponds to cleavage of amidic bond followed by possible decarboxylation and oxidation processes of organic fragments. The third stage decomposition takes place at 317-400^{0}C and highlights the rapid and progressive degradation of the organic residue until the metal oxide is obtained. The final products are CoO and some ash (20.27%, calcd. 21.09%).

Thermal decomposition of the nickel complex proceeds in two stages between 20-284^{0}C and 284-392^{0}C respectively (Figure 4d). First stage, with an endothermic peak at 175^{0}C, corresponds to the loss of water molecules inside the coordination sphere of the metal complexes. This phenomenon was achieved with an experimental mass loss of 6.67% (calcd. 6.91%). A strong exothermic effect was assigned to the total pyrolysis of metal complexes, a fact also found in the case of other metal complexes of amino acids or compounds with high percent of nitrogen [19, 32]. The final product is NiO and ash like the other metal complexes.

Figure 4d. TG-DTG-DTA diagram for the nickel complex (4)

29

The thermogram of manganese complex indicated four decomposition steps, occurred slowly like other Mn(II) complexes [23]. The first decomposition step, at temperature range 20-191^{0}C with an endothermic peak at 97^{0}C, corresponds to loss of water molecules outside of coordination sphere of complexes. The next three stages at temperature range 191-371^{0}C, 371-475^{0}C and 475-768^{0}C respectively, accompanied by exothermic peaks indicated the gradually decomposition of metal complex. The decomposition of the compound takes place progressively (Figure 4e), being probably accompanied by the breaking of the amidic bond, the destruction of the rest of the amine, oxidation or decarboxylation of the organic fragments leaving MnO and ash as a residue.

The decomposition of the compounds was not complete and the residue from 26.98% to 33.28% was observed, containing ash and metal oxide similarly to other compound with high nitrogen [17, 19, 32].
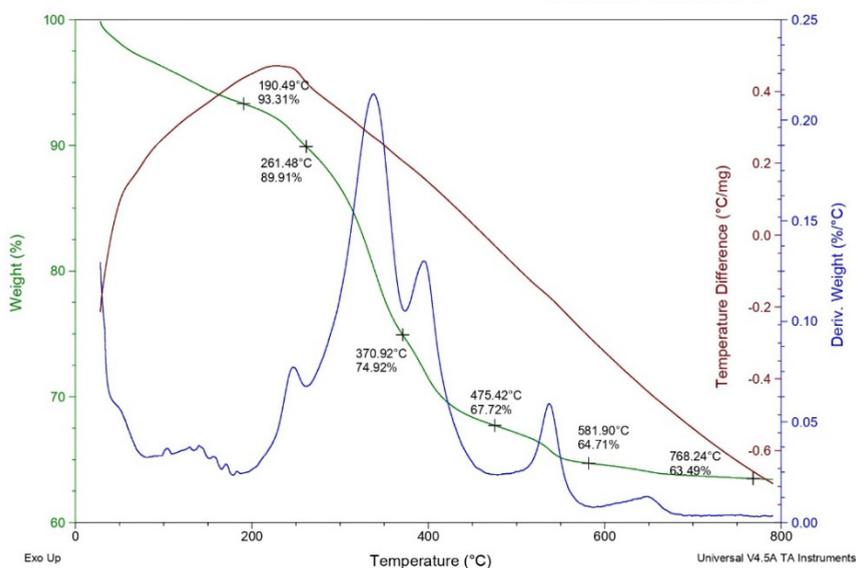

Figure 4e. TG-DTG-DTA diagram for the manganese complex (5)

EPR data

The EPR data are recorded at room temperature, in solid state, but just the cooper and manganese complexes provided relevant information, about the local symmetry found in compounds as a result of complexation. The experimental results are associated with the occurrence of paramagnetic Cu(II) for the compound (1).

The EPR spectrum of copper complex at room temperature, suggests the presence of CuN_2O_2 monomeric species. The shape of the spectrum corresponds to a S=1/2 system with rhombic **g** tensors. The principal values of **g** tensors (g_1=2.197, g_2=2.147 and g_3=2.051) indicate a rhombic distortion around the metallic ion (Figure 5).

The powder EPR spectrum of manganese complex is characterized by a quasi-isotropic **g** tensor ($\Delta B_{pp} \approx 400$ G) with the principal value g=2.074 due to the spin value of the CuN_2O_2 monomeric species [33-35].
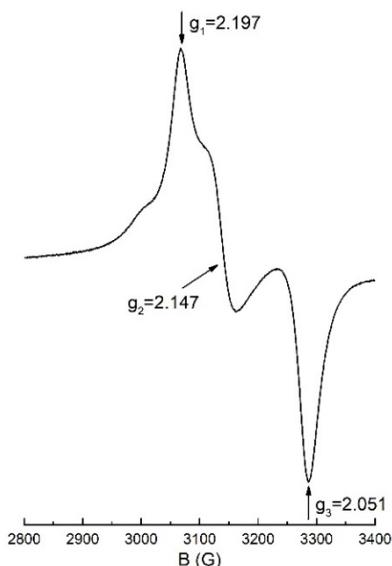
Figure 5. EPR spectrum of copper complex (2)

CONCLUSIONS

In this paper, we presented the syntheses and investigations of new transition metal complexes using β-L-aspartyl-cyclohexyl amide as ligand.

Elemental and thermal analysis lead to the idea that the ligand is anhydrous, but its metal complexes are hydrating. This phenomenon can be explained by the working conditions, in aqueous solutions, for the synthesis of metal complexes. The cooper and manganese complexes are hydrated with water molecules outside the coordination sphere, but for the cobalt and nickel complexes the water molecules are located inside the coordination sphere.

On the other hand, the $v(M-N)$ and $v(M-O)$ stretching bands in the metal complexes IR spectra support the complexation idea. The thermal stability of selected *3d* transition metal complexes indicated that all the compounds decompose in multistage in the temperature domain 20-800^{0}C.

For the cooper complex the EPR data indicates a rhombic distortion around the metallic ion.

The aspartyl amide acts as a bidentate ligand in all the metal complexes, coordination involving the carboxylate oxygen and the nitrogen atom belonging to the free amino group of the amino acid.

Based on thermal and spectroscopic data, it was found that metal complexes stability:

$[Mn(L)_2] \cdot 2H_2O < [Co(L)_2 \cdot 2H_2O] < [Ni(L)_2 \cdot 2H_2O] < [Cu(L)_2] \cdot H_2O$
obeys the Irving-Williams series [14,17,19].

The obtained data allows us to propose the following structural formulas for the studied transition metal complexes (Figure 6).

M = Co, Ni
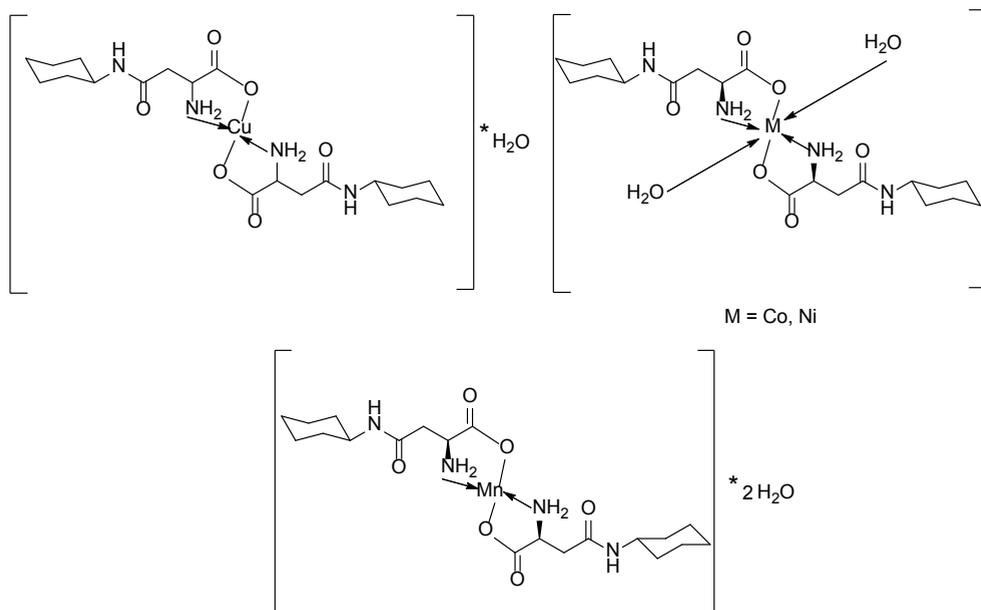
Figure 6. Suggested structures for the metal complexes

Since studies conducted with numerous organic ligands containing nitrogen and oxygen donor systems have demonstrated their antimicrobial activities or enzyme production inhibition, we propose that in the future, the new metal complexes synthesized by our team could be tested and find applications in

the medical field. Thermal analysis data have shown that the highest thermal stability is found in the case of the copper complex. On the other hand, the role of copper in numerous metabolic activities is well known, which could lead to promising results. Additionally, nickel, cobalt, and manganese are trace elements present in many biological systems, suggesting that their testing in the medical field should not be overlooked.

EXPERIMENTAL SECTION

Material and instrumentation

All reagents and chemicals were purchased from commercial sources and used as received. Melting points were measured on an ELECTROTHERMAL® instrument and were not corrected. CHNS analyses were determined on an elemental micro-analyzer Elementar vario MICRO Cube. Mass spectra were carried out on a LTQ ORBITRAP® XL (Thermo Scientific) instrument which was externally calibrated using the manufacturer's APCI or ESI(+) calibration mix. The samples were introduced into the spectrometer by direct infusion. IR spectra were recorded in KBr pellets on a JASCO® FT-IR 6200 Spectrometer which operates with $4cm^{-1}$ resolution. Thermogravimetry and differential thermal analysis (TG-DTG-DTA) curves were recorded with a Thermal Analyzer TA Instruments SDT Q600 V20.9 Build 20 on an interval of $20-800^0C$, at a heating rate of $10^0C/min$, in alumina crucibles and a dynamic air atmosphere. The ESR measurements were carried out on a Bruker Biospin EMX^{micro} spectrometer operating at X-band (9-10 GHz) with continuous wave at X-band (≈9 GHz). The spectra were recorded at room temperature with a microwave frequency of 9.4353 GHz, microwave power of 2 mW, modulation frequency of 100 kHz, modulation amplitude of 2 G.

General procedure for the synthesis of the metal complexes

The ligand namely (*S*)-2-amino-4-(cyclohexyl amino)-4-oxobutanoic acid (1 or HL) was prepared *via* a mild phthaloylation using the amide bond formation protocol [13].

Cu(II), Co(II), Ni(II) and Mn(II) complexes of the ligand were prepared by following a general method. The metal salt [$CuSO_4•5H_2O$, $CoSO_4•7H_2O$, $NiSO_4•7H_2O$ and $MnSO_4•4H_2O$] (1.30mmol) was dissolved in 7-8mL distilled water. The ligand (2mmol) was solved in a solution of Na_2CO_3 1M until pH = 11.0 – 11.5. To a solution of solved ligand was slowly added, continuously stirring, dropwise during 40 min., the solution of the metal salt at room temperature.

By adding the solution of metal ions, immediate color change was observed to the ligand solution, depending on the metal ion. The mixture was let to stir at the room temperature about 12h to perform the reaction. The final pH changed to 7.5-8.5 for all the compounds. The isolated solid complexes were obtained by vacuum filtration, washed with distilled water and finally dried in a vacuum desiccator for 72h.

Finally, the obtained compounds were subjected to elemental, spectroscopic and thermal investigations.

$C_{10}H_{18}N_2O_3$ (1 or HL): White solid; MW=214.2651; Mp=231-233^{0}C; Elemental Analysis(%) Calcd.(Found) C: 56.06(56.81), H: 8.47(8.11); N: 13.07(12.88); MS (ESI, CH_3OH) [M+H]: 215.2693; Exact Mass: 214.1317; FTIR (KBr,cm^{-1}): v_{max}: 3445, 3296, 2930, 2853, 1658, 1620, 1574, 1429, 1310; Thermal Analysis: T_{max}: 168^{0}C (Endo) (TG$_{exp}$=0.04%), 231^{0}C (Endo) and 272^{0}C (Exo) (TG$_{calcd}$=28.48%, TG$_{exp}$=29.25%, 339^{0}C (Exo), 356^{0}C (Exo) and 371^{0}C (Exo) (TG$_{calcd}$=25.69%, TG$_{exp}$=24.37%), 489^{0}C (Exo) and 570^{0}C (Exo) (TG$_{calcd}$=45.83%, TG$_{exp}$=46.34%), residue 45.83% (calcd) 46.43 (exp).

$C_{20}H_{36}CuN_4O_7$ (2): Pale-blue solid; MW=508.0684; Mp=312-314^{0}C (decomp.); Yield: 82%; Elemental Analysis(%) Calc.(Found) C: 47.28(47.98), H: 7.14(6.91), N: 11.03(11.29); MS (ESI, CH_3OH, without coordination water) [M+Na]: 512.1662; Exact Mass: 489.1774; FTIR (KBr,cm^{-1}): v_{max}: 3423, 3257, 2930, 2854, 1651, 1589, 1561, 1405, 1367, 588, 469; Thermal Analysis: T_{max}: 63^{0}C (Endo) (TG$_{exp}$=0.75%), 104^{0}C (Endo) (TG$_{calcd}$=3.54%, TG$_{exp}$=3.15%), 271^{0}C (Exo), 279^{0}C (Exo) and 296^{0}C (Exo) (TG$_{calcd}$=58.13%, TG$_{exp}$=56.32%), 392^{0}C (Exo) (TG$_{calcd}$=38.33%, TG$_{exp}$=39.78%), residue 38.33% (calcd) 39.78 (exp); EPR: (g$_1$=2.179, g$_2$=2.147, g$_3$=2.051); Molar Ratio Cu : L : H_2O = 1 : 2 : 1.

$C_{20}H_{38}CoN_4O_8$ (3): Pale-pink solid; MW=521.4709; Mp=273-275^{0}C (decomp.); Yield: 76%; Elemental Analysis(%) Calc.(Found) C: 46.06(46.78), H: 7.34(7.92), N: 10.74(11.03); MS (ESI, CH_3OH, without coordination water) [M+Na]: 508.1708; Exact Mass: 485.1810; FTIR (KBr,cm^{-1}): v_{max}: 3329, 3297, 2930, 2854, 1650, 1622, 1558, 1404, 1389, 531, 396; Thermal Analysis: T_{max}: 32^{0}C (Endo) (TG$_{exp}$=1.43%) 164^{0}C (Endo) (TG$_{calcd}$=6.90%, TG$_{exp}$=5.41%), 275^{0}C (Endo) (m.p.), 303^{0}C (Exo) (TG$_{calcd}$=42.90%, TG$_{exp}$=41.88%), 356^{0}C (Exo) (TG$_{calcd}$=29.93%, TG$_{exp}$=30.19%), residue 20.27% (calcd) 21.09% (exp); Molar Ratio Co : L : H_2O = 1 : 2 : 2.

$C_{20}H_{38}N_4NiO_8$ (4): Greenish-white solid; MW=521.2311; Mp=291-293^{0}C (decomp.); Yield: 76%; Elemental Analysis(%) Calc.(Found) C: 46.09(46.67), H: 7.35(7.78), N: 10.75(10.18); MS (ESI, CH_3OH, without coordination water) [M+Na]: 507.3627; Exact Mass: 484.1832; FTIR (KBr,cm^{-1}): v_{max}: 3339, 3295,

2936, 2854, 1650, 1573, 1588, 1418, 1312, 562, 423; Thermal Analysis: T_{max}: $175^{0}C$ (Endo) (TG_{calcd}=6.91%, TG_{exp}=6.88%), $360^{0}C$ (Exo) (TG_{calcd}=66.96%, TG_{exp}=65.79%), residue 26.13% (calcd) 27.33% (exp); Molar Ratio Ni : L : H_2O = 1 : 2 : 2.

$C_{20}H_{38}MnN_4O_8$ (5): Light-brown solid; MW 517.4758; Mp=238-240^{0}C (decomp.); Yield: 48%; Elemental Analysis(%) Calc.(Found) C: 46.42(45.93), H: 7.40(7.81), N: 10.83(11.04); MS (ESI, CH_3OH, without coordination water) [M+Na]: 504.3594; Exact Mass: 517.2070; FTIR (KBr,cm^{-1}): v_{max}: 3407, 2927, 2852, 1556, 1526, 1511, 1407, 1373, 457, 373; Thermal Analysis: T_{max}:97^{0}C (Endo) (TG_{calcd}=6.96%, TG_{exp}=6.69%), $243^{0}C$ (Exo), $354^{0}C$ (Exo) and $389^{0}C$ (Exo) (TG_{calcd}=24.93%, TG_{exp}=25.59%), $532^{0}C$ (Exo) and $643^{0}C$ (Exo) (TG_{calcd}=39.18%, TG_{exp}=36.51%), residue 28.93% (calcd) 26.98% (exp); EPR: g=2.07; Molar Ratio Mn : L : H_2O = 1 : 2 : 2.

REFERENCES

1. Y. M. Jamil; M. A. Al-Maqtari; F. M. Al-Azab; M. K. Al-Qadasy; A. A. Al-Gaadbi; *Eclet. Quim.,* **2018**, *43*(4), 11-24
2. M. Khuddus; M. Jayakannan; *Biomacromolecules*, **2023**, *24*, 2643-2660
3. Miller; A. Matera-Witkiewicz; A. Mikolajczyk; J. Watly; D. Wilcox, D. Witkowska; M. Rowinska-Zyrek; *Int. J. Mol. Sci.,* **2021**, *22*, 6971
4. Tomashevskii; O. A. Golovanova; S. V. Anisina; *Russ. J. Gen. Chem.,* **2021**, *91*(12), 2621-2626
5. N. Lihi; M. Lukacs; D. Szucs; K. Varnagy; I. Sovago; *Polyhedron*., **2017**, *133*, 364-373
6. M. Raics; D. Sanna; I. Sovago; C. Kallay; *Inorganica Chim. Acta*., **2015**, *426*, 99-106
7. T. O. Aiyelabola; D. A. Isabirye; E. O. Akinkunmi; O. A. Ogunkunle; I. A. O. Ojo; *J. Chem.,* **2016**, Article ID 7317015, https://doi.org/10.1155/2016/7317015
8. Nomiya; H. Yokoyama; *J. Chem.Soc., Dalton Trans*., **2002**, *12*, 2483-2490
9. D. Kalebic; K. Binnemans; P. A. M. de Witte; W. Dehaen; *RSC Sustainability,* **2023**, *1*, 1995-2005
10. Y. Hui; H. Qizhuang; Z. Meifeng; X. Yanming; S. Jingyi; *J. Chin. Rare Earth Soc.,* **2007**, 2, 150-156
11. X. Liu; M. Wu; C. Li; P. Yu; S. Feng; Y. Li; Q. Zhang; *Molecules*, **2022**, *27,* 2407
12. M. Patyal; K. Kaur; N. Gupta; R. Kaur; A. K. Malik; *Prot. Met. Phys. Chem*., **2023**, *59(2)*, 169-178
13. I. Abdiji; C. Sacalis; A. Shabani; A. Jashari; *J. Nat. Sci. Math.*, **2023**, *8(15-16)*, 72-81
14. H. Irving; R. J. P. Williams; *J. Chem. Soc.*, **1953**, 3192-3210

15. I. Sovago; E. Farkas; C. Bertalan; A. Lebkiri; T. Kowalik-Jankowska; H. Kozlowski; *J. Inorg. Biochem.*, **1993**, *51,* 715-726
16. L. Zapala; M. Kosinska; E. Woznicka; L. Byczynski; W. Zapala; *J. Therm. Anal. Calorim.*, **2016**, *124*, 363-374
17. C. Sacalis; F. Goga; C. Somesan; *Studia UBB Chemia*, **2018**, *63(4)*, 51-63
18. C. Sacalis; F. Goga; L. David; *Studia UBB Chemia*, **2017**, *62(4),* 181-192
19. C. Sacalis; S. Jahiji, A. Avram; *Studia UBB Chemia*, **2022**, *67(4)*, 337-352
20. M. Castillo; E. Ramirez; *Transit. Met. Chem.*, **1984**, *9*, 268-270
21. Z. K. Genc; S. Selcuk; S. Sandal; N. Colak; S. Keser; M. Sekerci; M. Karatepe; *Med. Chem. Res.*, **2014**, *23*, 2476-2485
22. P. S. Piispanen; P. M. Pihko; *Tetrahedron Lett.*, **2005**, *46*, 2751-2755
23. A. M. Hassan; B. H. Heakal; A. O. Said; W. M. Aboulthana; M. A. Abdelmoaz; *Egypt. J. Chem.*, **2020**, *63(7)*, 2533-2550
24. W. Ferenc; B. Cristovao; J. Sarzynski; P. Sadowski; *J. Therm. Anal. Calorim.*, **2012**, *110*, 739-748
25. I. Sakiyan; *Transit. Met. Chem.*, **2007**, *32*, 131-135
26. M. Tanaka; I. Yamashina; *Carbohydr. Res.*, **1973**, *27,* 175-183
27. K. Nakamoto; *Infrared and Raman Spectra of Inorganic and Coordination Compounds*, *Part. B: Applications in Coordination, Organometallic and Bioinorganic Chemistry*, John Wiley & Sons, Inc., Hoboken, New Jersey, Sixth Ed., **2009**, pp. 63-72
28. A. A. Osunlaja; N. P. Ndahil; J. A. Ameh; *Afr. J. Biotechnol.*, **2009**, *8(1)*, 4-11
29. O. F. Akinyele; A. B. Adesina; T. A. Ajayeoba; E. G. Fakola; *Sci. J. Chem.,* **2023**, *11(4)*, 137-145
30. T. H. Al-Noor; M. R. Aziz; A. T. AL-Jeboori; *J. Chem. Pharm. Res.*, **2014**, *6(4)*, 1225-1231
31. C. A. Terraza; L. H. Tagle; D. Munoz; A. Tundidor-Camba; P. A. Ortiz; D. Coll; C. M. Gonzalez-Henriquez; I. A. Jessop; *Polym. Bull.*, **2016**, *73*, 1103-1117
32. M. Worzakowska; M. Sztanke; K. Sztanke; *J. Therm. Anal. Calorim.,* **2022**, *147*, 14315-14327
33. L. D. Pinto; P. A. L. Puppin; V. M. Behring; D. H. Flinker; A. L. R. Merce; A. S. Mangrich; N. A. Rey; J. Felcman; *Inorganica Chim. Acta*, **2010**, *363*, 2624-2630
34. J. R. Pilbrow, *Transition ion electron paramagnetic resonance,* Clarendon Press, New York: Oxford University Press, **1990**, pp. 51-80
35. F. E. Mabbs; D. Collison; *Electron Paramagnetic Resonance of d Transition Metal Compounds,* Elsevier Science Publishers B.V. Amsterdam, Netherland, **2013**, pp. 83-124.